Plasmonics
https://doi.org/10.1007/s11468-024-02251-2

RESEARCH

Eco-Friendly Fabrication of Silver Nanoparticles for Sustainable Water Purification and Antibacterial Synergy

Parvathalu Kalakonda[1] · Mahesh Thodeti[1] · Cheguveera Ganneboina[1] · Keerthi Ankathi[1,2] · Swetha Kathri[1] · Karthik Begari[1,2] · Hruthik Sai Kante[1] · Vijendar Jupalli[1] · Yasaswi Khaderabad[3] · Saroj Vijaylaxmi[1] · Vijay Morampudi[3] · Pritam Mandal[4] · Vasudeva Reddy Yatham[1] · Imran Hasan[5] · Bala Bhaskar Podila[1]

Received: 26 January 2024 / Accepted: 20 February 2024

Abstract
Silver nanoparticles (AgNPs) were synthesized using the aqueous extract of *Terminalia chebula* (T-Chebula) fruits. Characterization through X-ray diffraction (XRD) and scanning electron microscopy (SEM) revealed AgNPs with a crystalline size ranging from 21 to 24 nm. The biosynthesized AgNPs exhibited a morphology unique to T-Chebula-AgNPs (TC-AgNPs), with an average size of 50 nm and a band gap energy of 2.8 eV. Evaluation of antimicrobial properties against *Escherichia coli* (*E. coli*) showcased the potential antibacterial activity of AgNPs compared to the standard gentamicin antibiotic. Notably, increasing concentrations of TC-AgNPs correlated with larger zones of inhibition, highlighting their efficacy. In contrast, the T-Chebula extract alone showed no bactericidal activity. Furthermore, under visible light irradiation, TC-AgNPs exhibited significant catalytic potential in degrading water-soluble industrial methylene (MB) dyes, achieving 92% dye degradation rate compared to the previous studies. The stability and recyclability of TC-AgNPs were notably robust across three iterations. Biogenically synthesized TC-AgNPs demonstrate exceptional potential in degrading organic pollutants and deactivating microorganisms. These findings underscore their promising applications in microbial control and the photodegradation of organic pollutants, highlighting their role in sustainable environmental remediation efforts.

Keywords Silver nanoparticles · Biosynthesis · Synergetic effect · Water purification · Antimicrobial activity

Introduction

Bionanotechnology, at the intersection of biology and nanotechnology, holds tremendous promise in the fields of antimicrobial activity and photocatalysis [1, 2]. This innovative approach leverages the unique properties of biological entities at the nanoscale to address pressing challenges in healthcare and environmental remediation [3, 4]. Specifically, the utilization of bio-inspired nanoparticles, such as those derived from plant fruits like *Terminalia chebula* fruit, showcases significant potential in both antimicrobial applications and photocatalysis [5, 6]. The rich phytochemical composition of *Terminalia chebula* fruit and other medicinal plants, fruits, including polyphenols, terpenes, and glycosides, contributes to the development of bio-nanomaterials with inherent antimicrobial and photocatalytic properties. These nanostructures not only exhibit high antibacterial efficacy but also serve as efficient photocatalysts, harnessing light energy to drive catalytic reactions for environmental decontamination. The emerging field of bionanotechnology, rooted in the principles of green chemistry, thus offers a sustainable and multifaceted approach to combating microbial infections and addressing environmental challenges through its unique antimicrobial and photocatalytic perspectives [7–13].

✉ Parvathalu Kalakonda
parvathalu.k@gmail.com

1 Department of Physics, Government City College (A), Nayapul, Osmania University, Hyderabad, Telangana, India 500002

2 Department of Physics, Pondicherry Central University, Pondicherry, India 605009

3 Department of Biochemistry, University of Hyderabad, Hyderabad, Telangana, India 500046

4 Department of Physics, Michigan Technological University, Houghton, MI 49931, USA

5 Department of Chemistry, College of Science, King Saud University, 11451 Riyadh, Saudi Arabia

Ayurveda, an ancient healing system rooted in Indian heritage, is esteemed as the "Mother of all healing," providing a global guide for modern drug exploration. T-Chebula fruit, a key element in Ayurveda, Unani, and Homoeopathic traditions, draws contemporary medical interest with its diverse phytochemical composition. The historical influence of T-Chebula fruit species in India spans over 3000 years, particularly in heart remedies [14]. Beyond its traditional applications for high cholesterol and digestive issues, T-Chebula exploration in HIV treatment and its role in a health-harmonizing blend indicate its multifaceted potential. Ongoing studies suggest T-Chebula oral administration alongside conventional medication may alleviate post-heart attack chest pain, while its fruit extract shows promise in antimicrobial and anti-inflammatory applications, including metal nanoparticle synthesis [15–20]. Complete understanding of *Terminalia*'s therapeutic potential calls for further research to explore.

Nanoparticles (NPs) are prevalent in various commercial products, emphasizing the importance of employing nature-based reducing and stabilizing agents in their production. This practice is crucial to mitigate toxicity and environmental hazards linked to conventional synthetic chemicals. Silver nanoparticles (AgNPs), widely incorporated into items such as home appliances, food packaging, electronics, textiles, and personal care products, serve to impart antimicrobial properties [21–24]. Their inclusion has demonstrated benefits such as extending the shelf life of perishable foods, promoting wound healing, and inhibiting bacterial growth [25–28]. Despite concerns about AgNPs' impact and accumulation in the environment, there is currently no established evidence of toxicity or adverse environmental effects [29–32]. Research findings generally support the advantages of AgNP use, but emphasize the need for a judicious, green approach to production, ensuring biodegradability and preventing bioaccumulation [33]. This sustainable method avoids generating hazardous waste associated with classical colloidal chemistry approaches [34–40].

Environmental pollution is one of the global problems that would suffer, and water pollution is a major challenge to resolve. Silver nanoparticles (AgNPs) offer significant advantages, including their potential to mitigate the accumulation of nonbiodegradable organic pollutants present in industrial effluents. Methylene blue (MB) dye, a common organic pollutant in industrial wastewater, poses a threat to aquatic life due to its persistence [41]. MB is a cationic dye commonly used in various industrial and medical applications, including textile dyeing, staining biological specimens, and as a medication for certain medical conditions. While MB is generally considered safe when used appropriately, it can pose health risks if exposure levels are excessive or prolonged [41–46]. The imperative of MB dye is to reduce its levels to meet safety standards in industrial effluent treatment and lead to the exploration of chemical degradation methods using sodium borohydride (NaBH4) [42]. Employing a catalyst is essential to expedite the reaction duration and align it with the rate of effluent discharge. AgNPs serve as effective catalysts, accelerating the degradation process. Recent studies highlight the catalytic degradation of MB dye using metal NPs synthesized through environmentally friendly methods [42–46]. However, the catalytic efficiency of nanoparticles is influenced by their shape and dimensions, prompting ongoing research to identify catalysts with enhanced performance. The major industrial wastewater loaded with different organic and inorganic pollutants (dyes). Dye wastewater has been discharging from industries such as textile, food, printing media, pharmaceutical industries, and leather industry. These dye materials change the purity of water beside it act as toxic effects. There are many methods that have been developed including chemical, biological, and physical process to clean water, but a few methods developed to remove dyes from the wastewater such as coagulation, filtration, adsorption, and oxidation. Recently, green synthesized hybrid composite photocatalyst materials has gained lot of attention due to its potential use in environmental treatment, cost-effective, non-toxic, and ecofriendly process [44–46]. Green synthesis route can significantly promote a new way that contributes in environmental sustainability.

In this study, we explore the utilization of T-Chebula fruit for eco-friendly green synthesis of silver nanoparticles (AgNPs). The focus is twofold: first, to assess their potential as a catalyst in the chemical reduction of MB dye and, second, to evaluate their antimicrobial activity against clinical pathogen *E. coli* bacteria. Our choice of T-Chebula fruit is grounded in its well-established benefits and widespread availability, making it an ideal candidate for large-scale, eco-friendly synthesis of AgNPs. The ultimate goal is to produce AgNPs that not only meet the criteria for inclusion in commercial products but also demonstrate efficacy as catalysts in the degradation of MB dye and the best nano-antibacterial agent to kill the pathogen bacteria.

Materials and Methods

Materials

We procured silver nitrate and solvents from Sigma-Aldrich, located in Bangalore, India. The T-Chebula fruits were meticulously collected from the herbal garden at Environmental Protection Training and Research Institute (EPTRI), Hyderabad.

Synthesis of Silver Nanoparticles (AgNPs)

The T-Chebula fruits were meticulously cleaned in a vial, subjected to several rinses with water to eliminate any dust particles. Afterward, the fruits were air-dried under ambient conditions and finely ground into a powder. Following this, 1.5 g of the TC fruit powder was combined with 75 ml of deionized (DI) water and stirred at 500 rpm while maintaining a temperature of 75 °C for 20 min. This process resulted in the T-Chebula fruit extract, which underwent filtration using filter paper.

For the synthesis of silver nanoparticles (TC-AgNPs), 75 ml of the T-Chebula fruit extract was slowly dispensed drop by drop (at a rate of one drop per second) from a burette into an 0.05 M $AgNO_3$ solution (conical flask). The addition of the fruit extract from the burette was carefully controlled as it dropped into the solution being stirred at 500 rpm, at a temperature of 80 °C. The process continued and was heated on a hot plate until a visible change in color was observed. Subsequently, the resulting solution underwent centrifugation at 3000 rpm for 20 min and was then dried in an oven at 60 °C to obtain the powdered TC-AgNP nanoparticles [39, 40]. We have optimized temperature and stirring conditions to synthesize high potential spherical AgNPs. A schematic representation of the TC-AgNP synthesis procedure is illustrated in Fig. 1.

Characterization of Synthesized TC-AgNPs

The confirmation of TC-AgNP formation involved ultraviolet–visible spectroscopy (UV–Vis), analyzing wavelengths in the range of 200 to 800 nm. The examination revealed characteristic absorption peaks associated with AgNPs. Additionally, Fourier Transform Infrared Spectroscopy (FTIR) was employed to identify specific functional phytochemical groups responsible for TC-AgNP formation, offering insights into the functional groups and vibrational chemical bonds that stabilize, reduce, and cap the nanoparticles. SEM was utilized to investigate the surface morphology, grain sizes, and size distribution of AgNPs. SEM provided visualizations of AgNPs, aiding in the determination of their surface size distribution. Furthermore, the crystal structure details of TC-AgNPs were explored using XRD, offering information about the nanoparticles' crystalline structure.

To summarize, the combination of UV–visible spectroscopy, FTIR, SEM, and XRD measurements collectively characterized the synthesized AgNPs, encompassing their optical properties, chemical composition, morphology, and crystal structure.

Antibacterial Activity

The evaluation of the antimicrobial activity of TC-AgNPs occurred in a sterile laboratory setting, utilizing a biosafety cabinet. All equipment and glassware employed for assessing antimicrobial activity underwent sterilization through autoclaving. To assess the antibacterial properties of the synthesized TC-AgNPs, experiments were conducted using enteropathogenic *Escherichia* (EPEC), with a reference antibiotic, gentamicin, serving as a comparative benchmark. In the following sections, we offer a concise overview of the

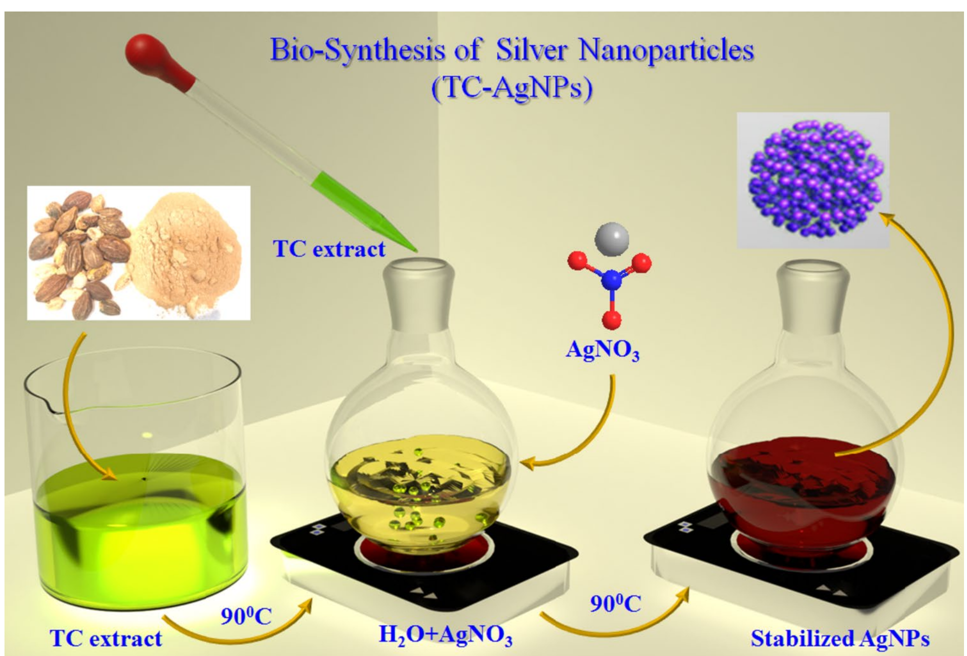

Fig. 1 Nucleation process of TC fruit extract-mediated TC-AgNPs

two methods utilized to appraise the antibacterial activity of the TC-AgNPs.

Bacterial Culture

Enteropathogenic *Escherichia coli* (EPEC: *E. coli*), characterized as a rod-shaped Gram-negative pathogen, underwent cultivation by reviving glycerol stocks stored at − 80 °C in Luria Bertani (LB) broth. The bacterial culture was nurtured at 37 °C for 12 to 14 h within a shaker incubator at 180 rpm. For the facilitation of growth and preparation for subsequent assays, the EPEC bacterial culture was streaked on LB agar plates. Following this, the overnight culture of EPEC with an optical density at 600 nm (OD 600 nm) of 1 was utilized in performing both the disc diffusion and minimum inhibitory concentration assays.

Disc Diffusion Assay Procedure

The antibacterial activity of TC-AgNPs at various concentrations (1–5%) was screened using the disc diffusion assay. The bacterial culture, grown overnight, was adjusted to 1×10^9 CFU/ml ($OD_{600} = 1.00$) in sterile LB broth. A 100 µl bacterial suspension was swabbed on sterile agar and allowed to dry. Filter paper discs, each containing 50 µl of different sample solutions (TC, Ag, AgNPs—1%, AgNPs—2%, AgNPs—3%, AgNPs—4%, AgNPs—5%), were placed on the LB agar surface and incubated inverted at 37 °C overnight. Subsequently, the zone of inhibition was measured. As positive control, 30 µg of gentamicin was used, while sterile LB broth served as the negative control. The antimicrobial activity of each concentration was quantified by the zone of inhibition (mm), with two replicates for each assay [48, 49].

Minimum Inhibition Concentration (MIC) Assay Procedure

Quantitative microspectrophotometric assay was employed to measure the antibacterial activity, with growth inhibition assessed at 600 nm in 96-well microtiter plates. Tests were conducted using 20 µl of TC-AgNPs at concentrations ranging from 1 to 5%, along with 10 µl of an overnight bacterial culture adjusted to a density of 1×10^9 CFU/ml ($OD_{600} = 1.00$) in sterile LB broth and 70 µl of LB broth. Microcultures containing 20 µl of sterile distilled water, replacing the test solution, served as a negative control. Additionally, 10 µl of 30 µg of gentamicin was used as the positive control. The plates underwent absorbance measurement at 600 nm in a 96-well plate reader. After 24 h of incubation at 37 °C, growth was recorded by measuring absorbance. The percentage growth was determined based on the relevant equation.

$$[(\Delta C - \Delta T)/\Delta C] \times 100$$

where ΔC is the corrected absorbance of the control microculture at 600 nm (24 h OD_{600} − 0 h OD_{600}) and ΔT corrected absorbance (24 h OD_{600} − 0 h OD_{600}) of test compound [49].

Photocatalytic Activity

To evaluate the photocatalytic activity of the synthesized TC-AgNPs in degrading methylene blue (MB) dye, a visible light source was employed as a substitute for natural sunlight. The reaction commenced with the addition of a 3-ml solution of TC-AgNPs (nanofluid catalyst) with a concentration of 10 mg/ml into a 40-ml dye solution with a concentration of 15 mg/ml. The resulting mixture was stirred in a darkroom for 20 min to establish the adsorption process. To monitor the progress of the reaction, samples were collected at 30-min intervals, and their absorption peaks were analyzed using UV–Vis spectroscopy. The initial UV–Vis spectra were obtained for the pristine MB dye, displaying characteristic bands at 630 nm and 430 nm wavelengths. Under visible light irradiation, the solution was continuously stirred, and 3 ml of suspension was withdrawn at 30-min intervals for up to 2 h to track changes in the dye absorption peak. Dye degradation was quantified using the following equation [39, 40], utilizing UV–Vis spectrum data.

$$\text{Degradation}(\%) = \left(\frac{A_0 - A_t}{A_0}\right) \times 100$$

where A_0 is the absorption at time 0; A_t is the absorption at time *t*.

Results and Discussion

UV–Vis Spectroscopy

The optical characteristics of nanoparticles are primarily influenced by factors such as surface morphology, particle size, dispersion quality, and shape. Notably, the colorless $AgNO_3$ precursor salt solution underwent a noticeable transformation, turning into a wine-red color as the T-Chebula fruit extract was gradually added dropwise into the precursor solution over approximately 30 min, indicating the formation of TC-AgNPs. In Fig. 2, the UV–Vis spectrum of TC-AgNPs spans from 300 to 750 nm, revealing a peak at 370 nm, which is characteristic of the surface plasmon resonance (SPR) of AgNPs. This phenomenon is attributed to the presence of electron-rich polyphenols in the fruit extract, which, in general, contribute electrons for the reduction of Ag^+ ions to AgNPs. The biocomponents present in the fruit

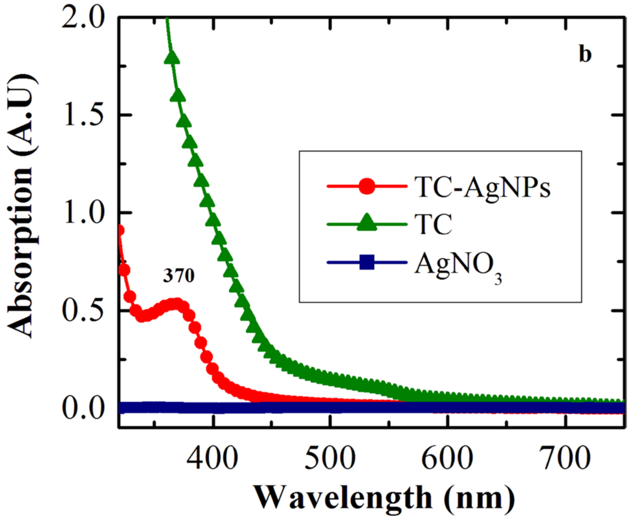

Fig. 2 UV–Vis absorption spectroscopy of TC-AgNPs showing peak absorbance

extract play a crucial role in synthesizing stable TC-AgNPs. The location of the absorption peak of TC-AgNPs is dependent on various factors, including reaction time, temperature, stirring, aqueous extract concentration, and precursor salt concentration.

Fourier Transform Infrared Spectroscopy (FTIR)

The FTIR analysis provides valuable insights into the functional groups and chemical bonds associated with TC-AgNPs. As illustrated in Fig. 3, the FTIR spectra of TC-mediated AgNPs reveal specific functional biomolecules that serve a dual purpose in reducing Ag^+ ions and stabilizing the resulting TC-AgNP nanoparticles. Comparative analysis with standard values aided in identifying surface functional groups. Peaks at 1305 cm^{-1} were attributed to -C–O–C- bands, 1634 cm^{-1} to the stretching vibration of C = C in the aromatic ring and C = O stretch in polyphenols. Simultaneously, bands at 2073 cm^{-1} were assigned to C–H stretch in alkanes and O–H stretch in carboxylic acid. Additionally, the peak at 3005 cm^{-1}, attributed to -C-H band, and 3315 cm^{-1}, signifying stretching vibrations of O–H groups in water, alcohol, and phenols, played a pivotal role in the synthesis and formation of AgNPs [45, 46].

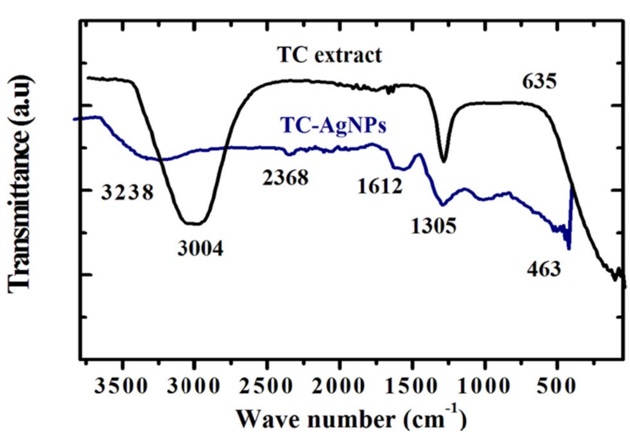

Fig. 3 FTIR spectrum of TC leaf extract-mediated AgNPs

The biocompounds, acting as electron donors, facilitate the reduction of Ag^+ ions and concurrently stabilize the evolving AgNP nucleation. The mechanism involves the coordination of Ag^+ ions with biocompounds via heteroatoms (O and N), accompanied by the transfer of electrons for the reduction of Ag^+ ions. The resulting Ag atoms serve as nucleation points, fostering further reduction and growth of the TC-AgNP nanoparticles. The FTIR spectrum of TC-AgNPs confirms the presence of phytochemicals, exhibiting vibrational bands at similar wavenumbers, indicative of their influential role in stabilizing the TC-AgNPs.

Scanning Electron Microscopy (SEM)

In Fig. 4a, b, the grain size and surface morphology characteristics of TC-AgNPs are illustrated. Micrograph images of TC-AgNPs reveal spherical shapes with sizes ranging from 20 to 100 nm, and the diameter distribution is presented in Fig. 4d. Analysis of the EDX profile data confirms the presence of TC-AgNPs, as indicated by a silver component signal. Furthermore, the EDX image in Fig. 4c shows substantiating the existence of oxygen and carbon compounds on the particle surface. These compounds are likely phytoconstituents from the fruit extract. The EDX data conclusively confirm the synthesis of TC-AgNPs using T-Chebula fruit extract. Despite interactions, individual TC-AgNPs are well dispersed without any aggregation, indicating the influence of phytochemicals and biocomponents in both the reduction and stabilization of TC-AgNPs in the colloidal solution. Notably, the absence of direct contact between TC-AgNPs can be attributed to the stabilizing action of capping agents present in the T-Chebula fruit extract. These phytochemicals actively participate in the reduction and stabilization processes of TC-AgNP nanoparticles.

Powder X-Ray Diffraction (XRD) Study of TC-AgNPs

XRD measurements, along with subsequent analysis, were employed to elucidate the details of the crystalline structure of TC-AgNPs. The XRD diffraction pattern of AgNPs clearly indicates a crystalline structure, as depicted in Fig. 5. Scherrer's formula was applied to estimate the crystalline size of AgNPs. The distinct peak intensities observed at 37.80, 43.90, 640, and 77.20 correspond to the (111), (200), (220), and (311) planes of the face-centered cubic lattice,

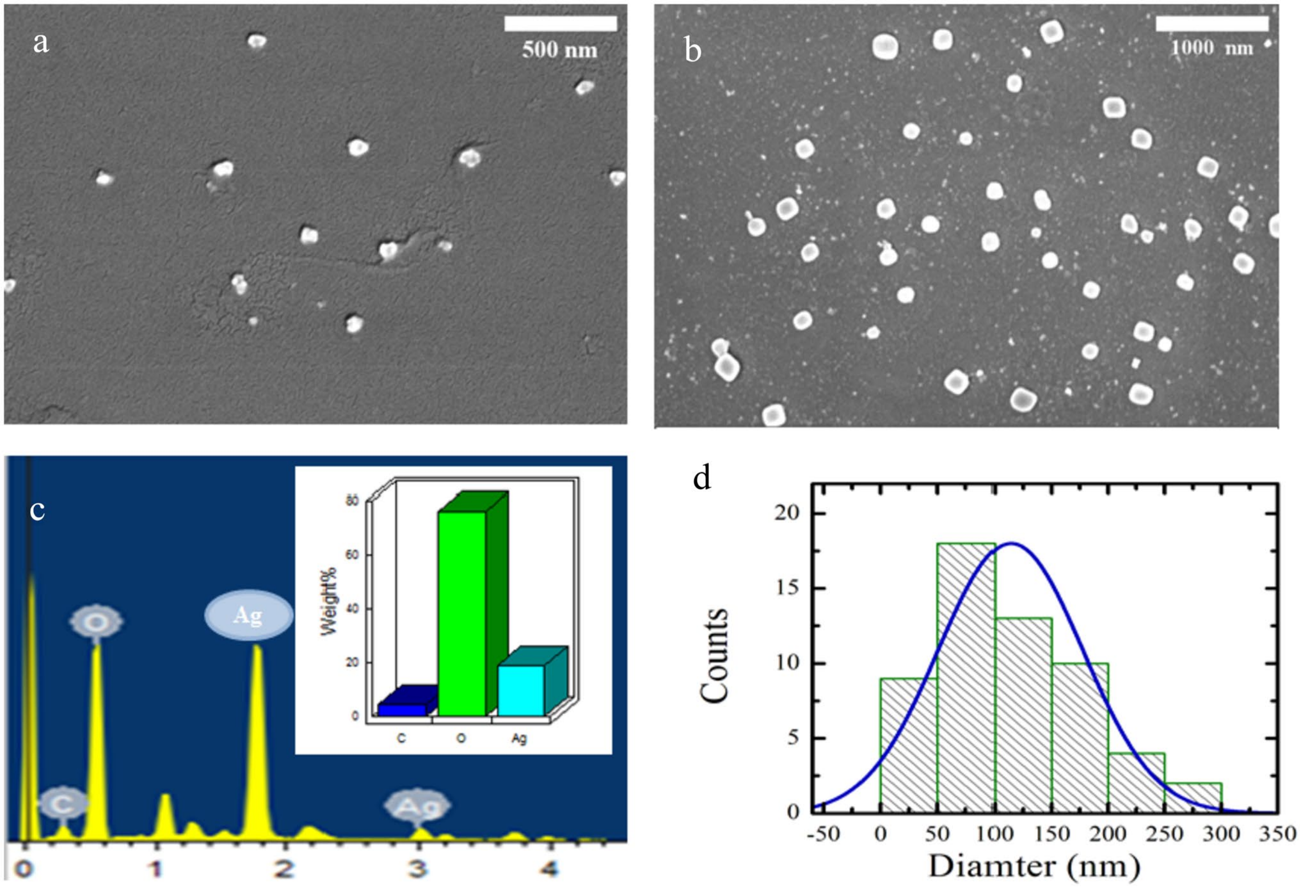

Fig. 4 SEM image of the **a**, **b** TC-AgNPs. **c** EDX spectrum of silver signal. **d** TC-AgNP size distribution

respectively, as established for TC-AgNPs according to JCPDS file no. 04–0783. This confirmation validates the crystalline phase of AgNPs and facilitates the measurement

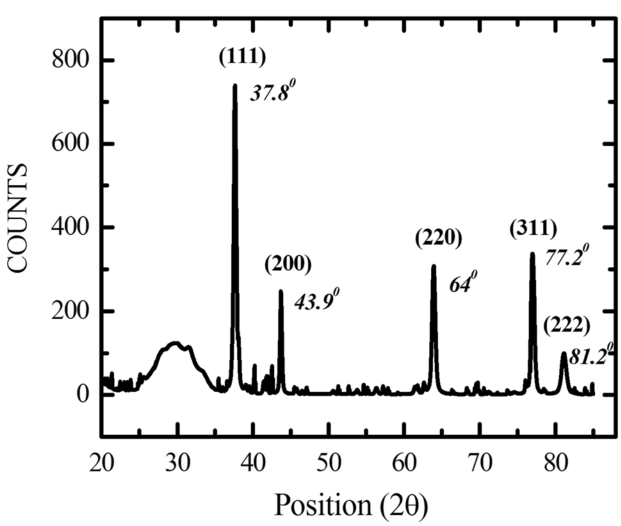

Fig. 5 Stacked XRD spectrum of TC-AgNPs

of the single crystalline size of AgNPs. The noteworthy peak at (111) is particularly significant, and the lattice parameters (2.6 nm) were calculated using Bragg's equation.

$$a = \lambda\left(\frac{h^2 + k^2 + l^2}{2\sin\theta}\right)A^0$$

The crystalline size of TC-AgNPs was computed utilizing Debye–Scherrer's equation ($D = 0.9\lambda/\beta\cos\theta$), where λ represents the wavelength of X-rays (0.154 nm), β denotes the full width at half maximum (FWHM), and θ signifies the angle of diffraction. The calculated crystalline size of TC-AgNPs was approximately 21–24 nm FCC structure. Comparable diffraction patterns have been reported for AgNPs synthesized using other plant extracts, and the structure of details are mentioned in Table 1.

Catalytic Degradation of MB Dye Using the TC-AgNPs

Figure 6 provides a visual representation of the photocatalytic effectiveness of TC-AgNPs in the degradation process of MB dye. The rate at which the dye degrades depends on

Table 1 Crystalline size for different planes of TC-AgNPs ($\lambda = 0.1541$ nm and $K = 0.9$)

S. No	Planes (hkl)	2θ (degree)	Sinθ (rad)	Cosθ (rad)	FWHM (β) (radians)	Interplanar spacing (d) (nm)	Lattice constant (a) (nm)	Cell volume (a^3)	Crystalline size (D) (nm)
1	111	37.8	0.05	0.99	0.0066	1.54	2.6	18.8	21.5
2	200	43.9	0.09	0.98	0.0052	0.86	1.7	5.1	27.4
3	220	64	0.55	0.83	0.0070	0.55	1.1	1.4	24.2

key factors, including the duration of irradiation, the light source employed, and the concentrations of both the dye and the catalyst. In our investigation, sunlight served as the primary driving force for the degradation process. The remarkable band gap and substantial surface area to volume ratio of TC-AgNPs significantly contribute to their catalytic efficiency in dye degradation.

Systematic sampling at specified time intervals post-exposure to light allowed for the characterization of the samples through UV–Vis spectroscopy analysis of absorption spectra. The presence of TC-AgNPs as a catalyst notably accelerated the reaction rate and substantially shortened the reaction time. The reduction in absorbance of the most intense peak at 661 nm, characteristic of MB dye, was monitored over time. The degradation of MB dye in the presence of TC-AgNPs peaked at 92% within 120 min, as evidenced by the decrease in absorbance (refer to Fig. 7) along with a corresponding high pseudo-first-order rate constant (Fig. 7). It is noteworthy that after achieving 92% degradation, the catalyst surface becomes saturated with the product, hindering further degradation. Additionally, the band gap energy was calculated using Tauc plots (see Fig. 7). This

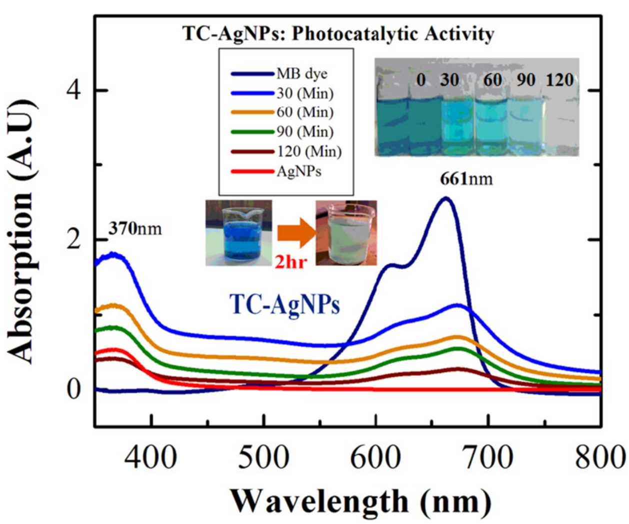

Fig. 6 Degradation of MB dye over TC-AgNPs nano-photocatalyst vs intensity change with irradiation time (25 µLt of MB dye in 50-ml DI water)

comprehensive study underscores the efficiency of TC-AgNPs as a catalyst in the photocatalytic degradation of MB dye under sunlight irradiation.

The optical band gap of TC-AgNPs, initially determined to be approximately 2.6–2.8 eV through UV data analysis, was subsequently confirmed using the Tauc relation and absorption spectrum, as depicted in Fig. 7. This considerable band gap highlights the promising potential of TC-AgNPs as photo-nanocatalysts for various applications. The wide band gap enables efficient utilization of visible light in catalytic processes, thereby enhancing their overall photocatalytic activity. This study emphasizes the prospective environmental applications of TC-AgNPs in the field of advanced materials science and catalysis. The observed optical energy band gap may be attributed to indirect interactions. It is crucial to acknowledge that the phytochemicals stabilizing TC-AgNPs play a role in attracting dye molecules to the AgNPs' surface through hydrophobic interaction and van der Waals forces. Our research findings revealed a decrease in the absorption band intensity with increasing duration of light exposure.

The degradation or decolorization of dyes is primarily ascribed to the action of oxygen radicals and hydroxyl radicals, both of which play a pivotal role in breaking down and neutralizing toxic contaminants present in the dye. With prolonged exposure to light, the color of MB dye gradually transitions into a lighter shade of blue or becomes colorless. The degradation efficiency for MB dye was quantified at approximately 92% for a 3-ml TC-AgNP nanocatalyst concentration, as illustrated in Fig. 8. This high degradation efficiency was achieved after approximately 2 h of exposure to a 10-W light source, utilizing 3 ml of the TC-AgNP photocatalyst compared to the previous studies [50–52].

Notably, a higher degradation rate was observed at the lower concentration of 3 ml of the TC-AgNP catalyst after 2 h, indicating an optimal catalyst concentration for the reduction process. This observation sheds light on the intricate dynamics involved in the photocatalytic degradation of dyes, providing valuable insights for further scientific mechanism (refer to Fig. 9).

The essential players in the detoxification of MB dye molecules under light were elucidated through the process of photocatalysis. Figure 9 provides a clear illustration of the proposed mechanism governing the photocatalytic

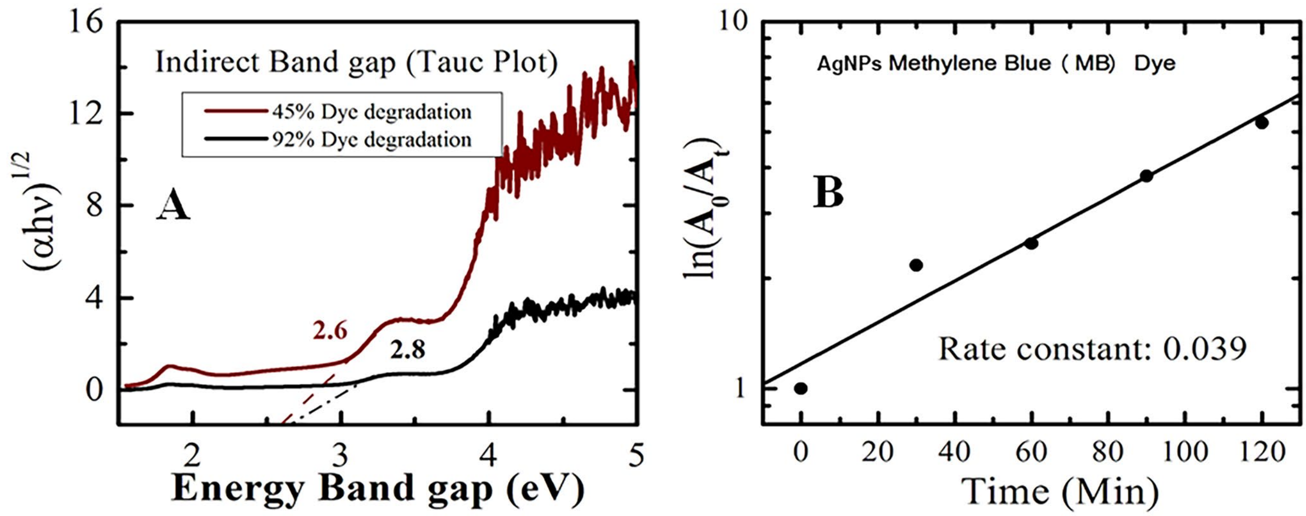

Fig. 7 **A** Calculation of optical band gap of nanocatalyst from UV–Vis data analysis. **B** Plot of ln (A_0/A_t) versus time

degradation of MB dye. TC-AgNPs, with a narrow band gap, serve as a crucial nanocatalyst in promoting the generation of electron–hole pairs. This is attributed to the minimal absorption energy required for electrons to transition from higher occupied orbit states to lower unoccupied orbit states.

Upon absorbing light energy, a nanocatalyst such as TC-AgNPs exhibits an absorption intensity that aligns with the band gap energy of the catalyst itself. The process of energy transition involves a shift from the ground state to the excited state, giving rise to several critical components, including a band gap, a valence band hole (h^+), a liberated electron (e^-), and a conduction band electron. Remarkably, the hole plays an important role as an attractive receptor for electrons from pollutants, thereby initiating their degradation.

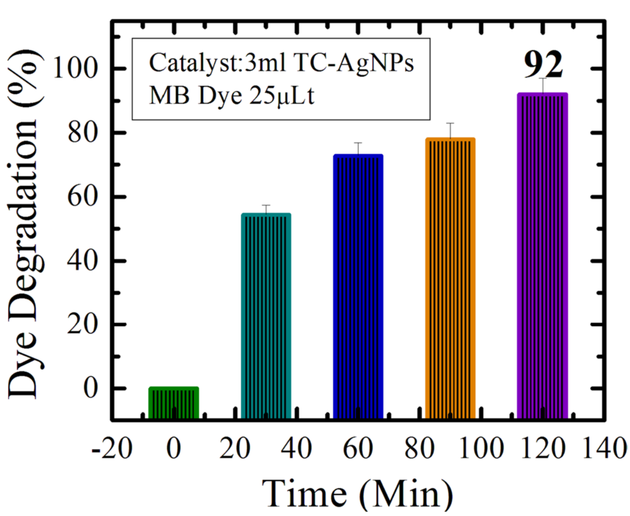

Fig. 8 Dye degradation % activity with TC-AgNP catalyst as the function of time

In this process, highly oxidizing species come into play, converting water molecules into hydroxyl radicals (OH), which play a vital role in degrading organic contaminants. Simultaneously, oxygen molecules combine with electrons, transforming into superoxide radicals (O_2). This intricate series of events illustrates the significance of TC-AgNPs as a photocatalyst in the generation of reactive species, contributing to the effective degradation of MB dye molecules.

The reduction of pollutants unfolds through the following sequence:

$$\text{Photocatalyst AgNPs} + h\nu \rightarrow e^- + h^+$$

$$\text{Photocatalyst AgNPs}(e^-) + O_2 \rightarrow O_2^-(\text{superoxide radical})$$

$$\text{Photocatalyst AgNPs}\left(h^+\right) + H_2O \rightarrow OH^-(\text{superoxide radical})$$

$$O_2^-(\text{or})OH^- + \text{Dye} \rightarrow \text{Degraded material}$$

This process offers valuable insights into the intricate pathways through which pollutants are effectively reduced, revealing the promising potential of these mechanisms in advanced environmental applications. The surface of TC-AgNPs is enriched with phenolic compounds and bioflavonoids derived from the T-Chebula fruit extract, playing a vital role in augmenting the generation of superoxide radicals from oxygen molecules and enhancing overall photocatalytic activity. Importantly, our findings confirm that oxide and hydroxyl radicals are indeed the predominant reactive species generated during the photocatalytic degradation of water-soluble dyes. This insight adds depth to

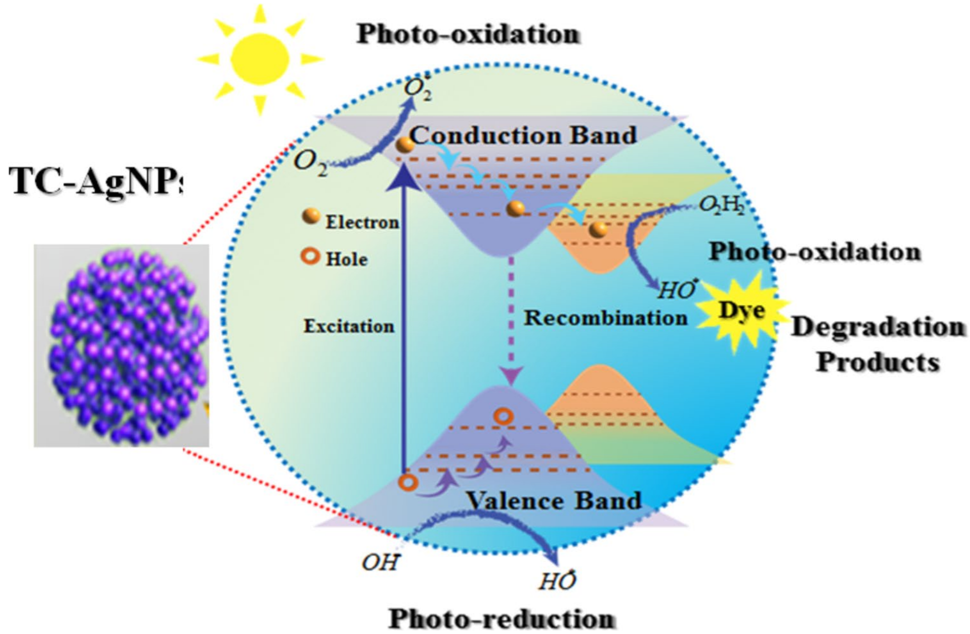

Fig. 9 Schematic representation of photocatalytic mechanism with TC-AgNPs

our understanding of the mechanistic intricacies underlying the photocatalysis process, emphasizing the potential of TC-AgNPs for advanced applications in environmental remediation.

With an increase in the concentration of the photocatalyst or at the optimum concentration (3 ml), there is a corresponding increase in the number of available reaction sites, leading to enhanced generation of electron–hole pairs. This, in turn, promotes the amplified production of hydroxyl radicals, essential for the efficient detoxification of organic pollutants. Additionally, the morphological characteristics and grain size of TC-AgNPs are pivotal factors affecting the efficacy of MB dye degradation. Catalyst nanoparticles with smaller sizes exhibit enhanced efficiency in dye degradation due to their ability to provide a higher quantity of active sites for dye absorption. In our investigations, noteworthy results were achieved by employing a 3-ml TC-AgNP catalyst. It is worth emphasizing that our AgNP catalyst was synthesized through a straightforward and environmentally friendly green synthesis process, utilizing TC fruit extract. This synthesis process demonstrated remarkable efficiency, achieving a 92% degradation rate for MB under standard visible light conditions. These results underscore the significant potential of TC-AgNPs as highly effective catalysts in various environmental applications.

Antibacterial Activity of TC-AgNPs

Disc Diffusion Assay

The antibacterial efficacy of TC-AgNPs, with varying concentrations of AgNP nanoparticles (1–5%), was evaluated against EPEC (*E. coli*) using the disc diffusion method. A significant distinction in the zone of inhibition was observed with different AgNP concentrations (1–5%) ($P < 0.05$), while no antibacterial activity was detected with *Tinospora cordifolia* (TC) fruit extract (Fig. 10). The recorded zone of inhibition, measured in millimeters, was plotted against AgNP concentration. A slight increase in the zone of inhibition was observed with higher AgNP concentrations, whereas TC extract did not kill any bacteria strain. The enhanced inhibitory and susceptibility effects of AgNPs against EPEC are ascribed to the presence of phytoconstituents on their surface, disrupting intracellular activities. Acting as stabilizing agents, phytochemicals facilitate seamless binding, interaction, and penetration of bacterial cells through hydrophobic and van der Waals forces. This interaction disrupts cellular activities by releasing Ag^+ ions, instigating reactive oxygen species, denaturing essential bacterial proteins, impeding DNA replication, damaging organelles, and inducing cytoplasmic leakage through cell membrane perforation.

Minimal Inhibitory Concentration (MIC) and Minimum Bactericidal Concentration (MBC)

The susceptibility of EPEC was assessed by determining the minimum inhibitory concentration (MIC) of TC-AgNPs, ranging from 1 to 5%. After a 24-h incubation period, turbidity was observed in T-Chebula untreated wells (growth control), indicating bacterial growth. Conversely, no turbidity was observed in wells treated with Ag and various concentrations of AgNPs (1 to 5%), demonstrating effective inhibition of bacterial growth (Fig. 11). To establish the minimum bactericidal concentration (MBC), 10 µl of

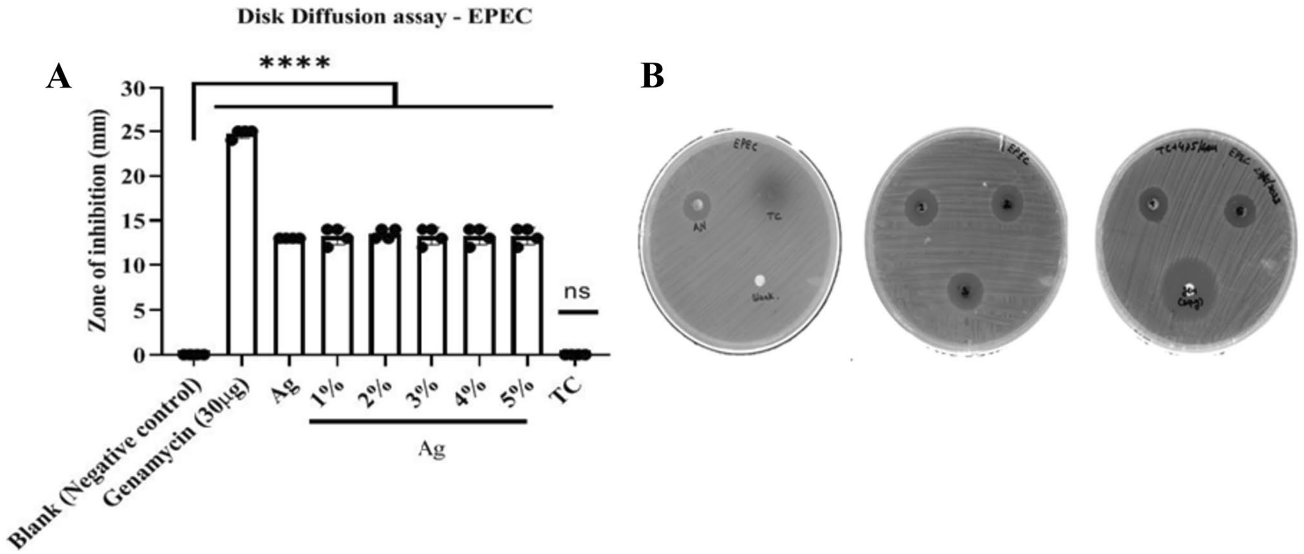

Fig. 10 **A** Antibacterial activity of the TC-AgNPs against EPEC. **B** Zone of inhibition produced by *TC-AgNPs* against various bacterial strains. D/W (distilled water); AgNP nanoparticles; TC—*Tinospora cordifolia*; 1—1% AgNPs; 2—2% AgNPs; 3—3% AgNPs; 4—4% AgNPs; 5—5% AgNPs; Gen—gentamycin 30 µg (positive control); Blank—LB broth (negative control)

the suspension was inoculated on LB agar and incubated overnight. No growth was observed in AgNP samples and varying concentrations of AgNPs from 1 to 4%, indicating a bactericidal effect. However, growth was observed at AgNPs-5%, suggesting a bacteriostatic effect at this concentration. The details are shown in Table 2 and statistical analysis using one-way ANOVA yielded a significant result ($P < 0.0001$) for MIC.

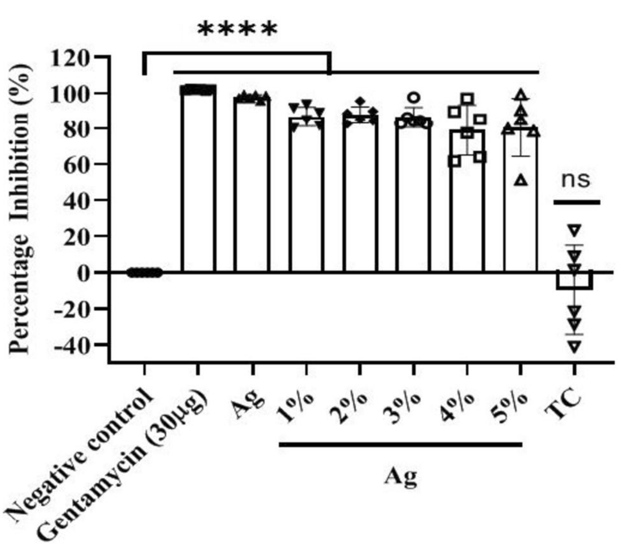

Fig. 11 The minimum inhibitory concentration (MIC) against EPEC after incubation for 24 h at 37 °C *TC-AgNPs* (concentration varied from 1 to 5%). Data are expressed as means ± SD. Statistical analysis was performed by one-way ANOVA ($P = < 0.0001$) with respect to negative control ($n = 6$)

The antimicrobial effectiveness of TC-AgNPs was assessed against enteropathogenic *E. coli*, comparing it to the standard reference antibiotic gentamicin, well known for its efficacy against this strain. The results unequivocally demonstrated that the synthesized TC-AgNPs exhibited significantly higher antimicrobial activity against enteropathogenic *E. coli*, highlighting their potential as potent antimicrobial agents. These findings align with prior studies emphasizing the advantages of AgNP nanoparticles, showcasing enhanced physicochemical properties and heightened antimicrobial effectiveness. The superior antibacterial activity of TC-AgNPs can be attributed to the synergistic effects resulting from the incorporation of metal ions, contributing to an overall enhancement in antimicrobial efficacy. To elucidate the potential mechanisms behind this heightened antibacterial activity, Fig. 12 illustrates four plausible interactions between TC-AgNPs and *E. coli* pathogenic cells [51, 52]. These mechanisms include TC-AgNPs adhering to the bacterial cell surface and disrupting the cell membrane, TC-AgNPs infiltrating the bacterial cell membrane and interacting with cellular organelles, TC-AgNPs triggering an increase in reactive oxygen species (ROS) within the cell membrane, leading to cell damage, and finally, TC-AgNPs modulating the cellular signaling system, ultimately deactivating the cells and resulting in cell death [47, 52–57].

Our study underscores the utilization of T-Chebula fruit extracts as a robust and environmentally friendly resource for

Table 2 The details of minimum bactericidal concentration (MBC) by inoculating 10 µl of *TC-AgNPs* (ranging from 1 to 5%) on sterile LB agar plates and incubated for overnight at 37 °C ($n = 6$)

Sample	Ag	TC	Ag-1%	Ag-2%	Ag-3%	Ag-4%	Ag-5%	Gentamycin (30 µg)	Growth control
	−	+	−	−	−	−	+	−	+

+ = presence of growth; − = absence of growth

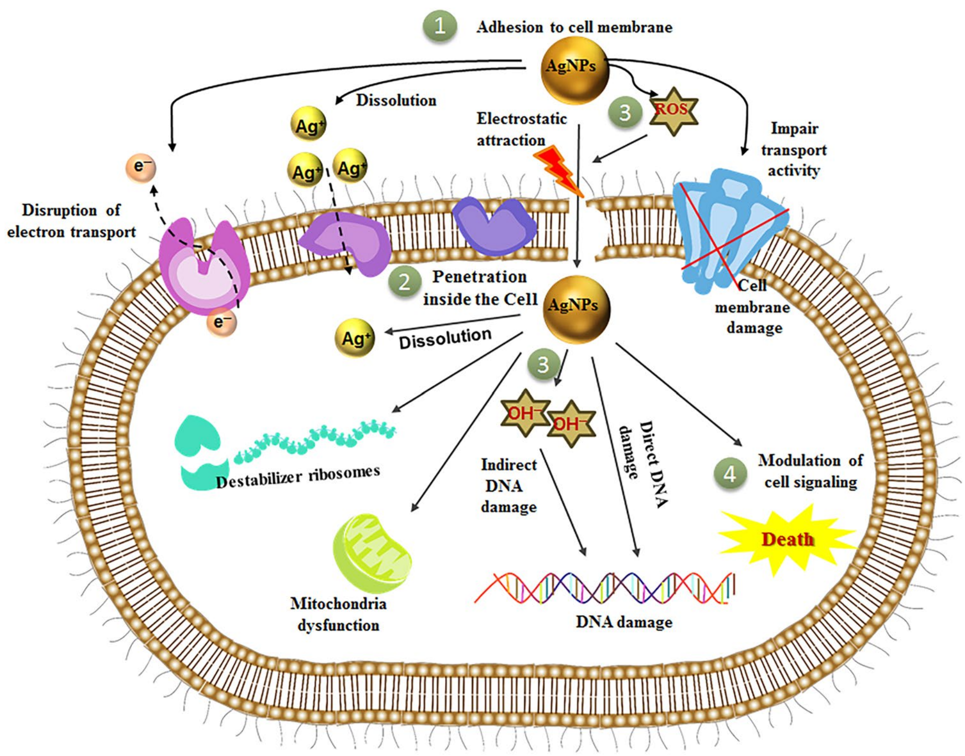

Fig. 12 The possible mechanism routes of antibacterial action of TC-AgNP nanoparticles

green synthesis, yielding high-quality TC-AgNPs. Leveraging its rich mineral and vitamin content, the plant extract demonstrated remarkable efficiency as a capping, reducing, and stabilizing agent. These findings are in line with recent studies advocating for the potential of biogenic AgNPs combined with phytochemicals in treating chronic infections. In the face of escalating multidrug-resistant microbes, our research highlights the pressing need for non-toxic antibacterial agents to combat microbial infections. Green-synthesized nanoparticles present a sustainable and eco-friendly alternative, steering clear of the use of hazardous chemicals. We emphasize the therapeutic potential of TC-AgNPs in addressing chronic infections, underscoring the importance of further in vitro and in vivo studies for validation.

Conclusion

Our study successfully synthesized silver nanoparticles (AgNPs) using a biosynthesis method with T-Chebula fruit extract, showcasing their remarkable potential in various applications. Characterization through XRD and SEM analysis revealed well-defined FCC structure with a crystalline size of 21–24 nm, while the biosynthesized morphology displayed an average size of 50 nm and a band gap energy of 2.8 eV. These TC-AgNPs exhibited potent antibacterial activity against *E. coli* bacteria, demonstrating significant synergistic effects. Notably, higher concentrations of TC-AgNPs led to a slight increase in the zone of inhibition, while the T-Chebula fruit extract alone showed no antibacterial activity. Furthermore, our study highlighted the photocatalytic dye degradation activity of TC-AgNPs under visible light irradiation, particularly in degrading water-soluble industrial methylene blue (MB) dyes, achieving an impressive 92% dye degradation rate. This efficacy surpassed previous studies, indicating the promising catalytic potential of TC-AgNPs in environmental remediation. Overall, the biogenically synthesized TC-AgNPs exhibit outstanding antibacterial capabilities and significant promise in degrading organic pollutants, positioning them as versatile and environmentally friendly materials. These findings underscore their potential applications in microbial control and efficient photodegradation of organic pollutants, contributing to sustainable and impactful research in water purification. Our ongoing studies aim to further explore the control of different dye types and concentrations using our nanocatalyst, extending the scope and applicability of TC-AgNPs in environmental remediation efforts.

Acknowledgements 1. The authors would like to thank the Department of Physics at Government City College for their support in completing this project. 2. The authors also extend their thanks to Researchers Supporting Project (Ref;RSPD2024R670), King Saud University, Riyadh, Saudi Arabia.

Author Contribution Parvathalu Kalakonda: Supervision, writing-original draft and editing, visualization Mahesh Thodeti, Cheguveera Ganneboina, Saroj Vijaylaxmi, Keerthi Ankathi, Swetha Kathri, Karthik Begari, Hruthik Sai Kante, Vijendar Jupalli, : Designing experiment, and Data collection, Yasaswi Khaderabad & Vijay Morampudi: Designing experiment procedure and investigation antibacterial activity Vasudeva Reddy Yattam, Bala Bhaskar Podila, Imran, Hasan & Pritam Mandal: Review of articles and data analysis.

Funding No funding was received for this project.

Data Availability No datasets were generated or analyzed during the current study.

Declarations

Ethical Approval Internal review board committee of our lab states that we do not have any consent to publish this antimicrobial and other data.

Competing Interest The authors declare no competing interests.

References

1. Ahmad J et al (2016) Differential cytotoxicity of copper ferrite nanoparticles in different human cells. J Appl Toxicol 36(10):1284–1293
2. He HM et al (2022) Metal-organic framework supported Au nanoparticles with organosilicone coating for high-efficiency electrocatalytic N2 reduction to NH3. Appl Catal B-Environ 302
3. Ijaz I, Gilani E, Nazir A, Bukhari A (2020) Detail review on chemical, physical and green synthesis, classification, characterizations and applications of nanoparticles. Green Chem Lett Rev 13(3):223–245
4. Weiss C, Carriere M, Fusco L, Capua I, Regla-Nava JA, Pasquali M, Delogu LG (2020) Toward nanotechnology-enabled approaches against the COVID-19 pandemic. ACS Nano 14(6): 6383–6406
5. Devi D, Julkapli NM, Sagadevan S, Johan MR (2023) Eco-friendly green synthesis approach and evaluation of environmental and biological applications of Iron oxide nanoparticles. Inorganic Chem Commun 110700
6. Ogundare SA, Adesetan TO, Muungani G, Moodley V, Amaku JF, Atewolara-Odule OC, van Zyl WE (2023) Catalytic degradation of methylene blue dye and antibacterial activity of biosynthesized silver nanoparticles using Peltophorum pterocarpum (DC.) leaves. Environ Sci: Adv 2(2):247–256
7. Sahooli M, Sabbaghi S, Saboori R (2012) Synthesis and characterization of mono sized CuO nanoparticles. Mater Lett 81:169–172
8. Das SS et al (2020) Stimuli-responsive polymeric nanocarriers for drug delivery, imaging, and theragnosis. Polymers 12(6)
9. Chu YM et al (2021) Enhancement in thermal energy and solute particles using hybrid nanoparticles by engaging activation energy and chemical reaction over a parabolic surface via finite element approach. Fractal Fract 5(3)
10. Mohammad M, Seyedeh NA, Mohsen M, Davood KN, Nima F (2024) Stevia rebaudiana leaf extract mediated green synthesis of cerium oxide nanoparticles for antibacterial activity and photocatalytic degradation of tetracycline, desalination and water treatment 100126
11. Wang YG et al (2016) Experimental evaluation of the lubrication properties of the wheel/workpiece interface in minimum quantity lubrication (MQL) grinding using different types of vegetable oils. J Clean Prod 127:487–499
12. Guo SM et al (2017) Experimental evaluation of the lubrication performance of mixtures of castor oil with other vegetable oils in MQL grinding of nickel-based alloy. J Clean Prod 140:1060–1076
13. Wang YG et al (2016) Experimental evaluation of the lubrication properties of the wheel/workpiece interface in MQL grinding with different nanofluids. Tribol Int 99:198–210
14. Koehn FE, Carter GT (2005) The evolving role of natural products in drug discovery. Nat Rev Drug Discov 4:206–220
15. Kumar KM, Mandal BK, Sinha M, Krishnakumar V (2012) Terminalia chebula mediated green and rapid synthesis of gold nanoparticles. Spectrochim Acta Part A Mol Biomol Spectrosc 86:490–494
16. Espenti CS, Rao KK, Rao KM (2016) Bio-synthesis and characterization of silver nanoparticles using Terminalia chebula leaf extract and evaluation of its antimicrobial potential. Mater Lett 174:129–133
17. Yatish KV, Prakash RM, Ningaraju C, Sakar M, Geetha-Balakrishna R, Lalithamba HS (2021) Terminalia chebula as a novel green source for the synthesis of copper oxide nanoparticles and as feedstock for biodiesel production and its application on diesel engine. Energy 215:119165
18. Ankegowda VM, Kollur SP, Prasad SK, Pradeep S, Dhramashekara C, Jain AS, Shivamallu C (2020) Phyto-mediated synthesis of silver nanoparticles using Terminalia chebula fruit extract and evaluation of its cytotoxic and antimicrobial potential. Molecules 25(21):5042
19. Kumar KM, Mandal BK, Kumar KS, Reddy PS, Sreedhar B (2013) Biobased green method to synthesise palladium and iron nanoparticles using Terminalia chebula aqueous extract. Spectrochim Acta Part A Mol Biomol Spectrosc 102:128–133
20. Tharani M, Rajeshkumar S, Al-Ghanim KA, Nicoletti M, Sachivkina N, Govindarajan M (2023) Terminalia chebula-assisted silver nanoparticles: biological potential, synthesis, characterization, and ecotoxicity. Biomedicines 11(5):1472
21. Karade VC, Patil RB, Parit SB, Kim JH, Chougale AD, Dawkar VV (2021) Insights into shape-based silver nanoparticles: a weapon to cope with pathogenic attacks. ACS Sustain Chem Eng 9(37):12476–12507
22. Benn T, Cavanagh B, Hristovski K, Posner JD, Westerhoff P (2010) The release of nanosilver from consumer products used in the home. J Environ Qual 39(6):1875–1882
23. Kessler R (2011) Engineered nanoparticles in consumer products: understanding a new ingredient
24. Cascio C, Geiss O, Franchini F, Ojea-Jimenez I, Rossi F, Gilliland D, Calzolai L (2015) Detection, quantification and derivation of number size distribution of silver nanoparticles in antimicrobial consumer products. J Anal At Spectrom 30(6):1255–1265
25. Kalakonda P (2016) Synthesis of silver nanowires for highly conductive and transparent films. Nanomater Nanotechnol 6
26. Kalakonda P, Sreenivas B (2017) Synthesis and optical properties of highly stabilized peptide-coated gold nanoparticles. Plasmonics 12(4):1221–1225

27. Kalakonda P, Banne S (2018) Synthesis and optical properties of highly stabilized peptide-coated silver nanoparticles. Plasmonics 13(4):1265–1269
28. Kalakonda P et al (2017) Microfibrous silver-coated polymeric scaffolds with tunable mechanical properties. RSC Adv 7(55):34331–34338
29. Hashemi N et al (2021) Leishmanicidal activities of biosynthesized BaCO3 (witherite) nanoparticles and their biocompatibility with macrophages. Bioprocess Biosyst Eng 44(9):1957–1964
30. Ren SC et al (2022) Well-defined coordination environment breaks the bottleneck of organic synthesis: Single-atom palladium catalyzed hydrosilylation of internal alkynes. Nano Res 15(2):1500–1508
31. Gao T et al (2020) Surface morphology assessment of CFRP transverse grinding using CNT nanofluid minimum quantity lubrication. J Cleaner Product 277
32. Yang M et al (2019) Predictive model for minimum chip thickness and size effect in single diamond grain grinding of zirconia ceramics under different lubricating conditions. Ceram Int 45(12):14908–14920
33. Song JY, Kim BS (2009) Rapid biological synthesis of silver nanoparticles using plant leaf extracts. Bioprocess Biosyst Eng 32(1):79–84
34. Vigneshwaran N et al (2007) Biological synthesis of silver nanoparticles using the fungus Aspergillus flavus. Mater Lett 61(6):1413–1418
35. Kalishwaralal K et al (2010) Biosynthesis of silver and gold nanoparticles using Brevibacterium casei. Colloids and Surfaces B-Biointerfaces 77(2):257–262
36. Kharissova OV et al (2013) The greener synthesis of nanoparticles. Trends Biotechnol 31(4):240–248
37. Bosetti M et al (2002) Silver coated materials for external fixation devices: in vitro biocompatibility and genotoxicity. Biomaterials 23(3):887–892
38. Kalakonda P, Thudumu S, Mynepally S et al (2023) Engineering micro/nano-fibrous scaffolds with silver coating for tailored wound repair applications. J Nanopart Res 25:254
39. Kalakonda P, Kumar DN, Rajitha K et al (2023) Facile synthesis of silver nanoparticles using green tea leaf extract and evolution of antibacterial activity. Plasmonics 18:1837–1845
40. Kalakonda P, Chinmayee S, Preethi B et al (2023) Green synthesis of silver nanoparticles using *Argyreia nervosa* leaf extract and their antimicrobial activity. Plasmonics 18:1075–1081
41. Khan S, Singh S, Gaikwad S, Nawani N, Junnarkar M, Pawar SV (2020) Optimization of process parameters for the synthesis of silver nanoparticles from Piper betle leaf aqueous extract, and evaluation of their antiphytofungal activity. Environ Sci Pollut Res 27:27221–27233
42. Anchan S, Pai S, Sridevi H, Varadavenkatesan T, Vinayagam R, Selvaraj R (2019) Biogenic synthesis of ferric oxide nanoparticles using the leaf extract of Peltophorum pterocarpum and their catalytic dye degradation potential. Biocatal Agric Biotechnol 20:101251
43. Hadi AA, Ng JY, Shamsuddin M, Matmin J, Malek NANN (2022) Green synthesis of silver nanoparticles using Diplazium esculentum extract: catalytic reduction of methylene blue and antibacterial activities. Chem Pap 76:65–77
44. Kalakonda P, Rajitha K, Chandrashekar B et al (2023) Biomimetic synthesis of copper nanoparticles using Tinospora cordifolia plant leaf extract for photocatalytic activity applications. Plasmonics
45. Kalakonda P, Bashitangu A, Mandal P (2024) Sarvani Jowhar Khanam, Murali Banovath, Imran Hasan, Bala Bhaskar Podila, Sustainable solutions for clean water: green synthesized Cu-Ag-Bimetallic nanoparticles based nano catalyst. Mater Sci Eng, B 301:117147
46. Sanjay P, Deepa K, Madhavan J, Senthil S (2018) Performance of TiO2 based dye-sensitized solar cells fabricated with dye extracted from leaves of Peltophorum pterocarpum and Acalypha amentacea as sensitizer. Mater Lett 219:158–162
47. Selvaraj R, Pai S, Murugesan G, Pandey S, Bhole R, Gonsalves D, Vinayagam R (2021) Green synthesis of magnetic α–Fe2O3 nanospheres using Bridelia retusa leaf extract for Fenton-like degradation of crystal violet dye. Appl Nanosci 11(8):2227–2234
48. Mohamed-Salem R, Rodríguez Fernández C, Nieto-Pelegrín E, Conde-Valentin B, Rumbero A, Martinez-Quiles N (2019) Aqueous extract of Hibiscus sabdariffa inhibits pedestal induction by enteropathogenic E. coli and promotes bacterial filamentation in vitro. Plos one 14(3)e0213580
49. Mohamed EAA, Muddathir AM, Osman MA (2020) Antimicrobial activity, phytochemical screening of crude extracts, and essential oils constituents of two Pulicaria spp. growing in Sudan. Sci Rep 10(1):1–8
50. Kalakonda P, Mandal P, Laxmi Mynepally S et al (2024) Comparison of multi-metallic nanoparticles-alternative antibacterial agent: understanding the role of their antibacterial properties. J Inorg Organomet Polym. https://doi.org/10.1007/s10904-023-02960-x
51. Chirumamilla P, Dharavath SB, Taduri S (2023) Eco-friendly green synthesis of silver nanoparticles from leaf extract of *Solanum khasianum*: optical properties and biological applications. Appl Biochem Biotechnol 195:353–368
52. Alzubaidi AK, Al-Kaabi WJ, Ali AA, Albukhaty S, Al-Karagoly H, Sulaiman GM, Asiri M, Khane Y (2023) Green synthesis and characterization of silver nanoparticles using *flaxseed* extract and evaluation of their antibacterial and antioxidant activities. Appl Sci 13:2182. https://doi.org/10.3390/app13042182
53. Khane Y, Benouis K, Albukhaty S, Sulaiman GM, Abomughaid MM, Al Ali A, Aouf D, Fenniche F, Khane S, Chaibi W et al (2013) Green synthesis of silver nanoparticles using aqueous *Citrus limon* zest extract: characterization and evaluation of their antioxidant and antimicrobial properties. Nanomaterials 2022:12
54. El-Khawaga AM, Elsayed MA, Gobara M et al (2023) Green synthesized ZnO nanoparticles by Saccharomyces cerevisiae and their antibacterial activity and photocatalytic degradation. Biomass Conv Bioref
55. El-Khawaga AM, Tantawy H, Elsayed MA et al (2022) Synthesis and applicability of reduced graphene oxide/porphyrin nanocomposite as photocatalyst for waste water treatment and medical applications. Sci Rep 12:17075
56. El-Khawaga AM, Elsayed MA, Fahim YA et al (2023) Promising photocatalytic and antimicrobial activity of novel capsaicin coated cobalt ferrite nanocatalyst. Sci Rep 13:5353
57. Elbasuney S, El-Khawaga AM, Elsayed MA et al (2023) Enhanced photocatalytic and antibacterial activities of novel Ag-HA bioceramic nanocatalyst for waste-water treatment. Sci Rep 13:13819
58. Abd Elkodous M, El-Sayyad GS, Youssry SM et al (2020) Carbon-dot-loaded $Co_xNi_{1-x}Fe_2O_4$; $x = 0.9/SiO_2/TiO_2$ nanocomposite with enhanced photocatalytic and antimicrobial potential: an engineered nanocomposite for wastewater treatment. Sci Rep 10: 11534